

# Quantifying dynamical and structural invariance in a simple molten salt model

Cite as: J. Chem. Phys. 155, 054506 (2021); doi: 10.1063/5.0055794

Submitted: 3 May 2021 • Accepted: 2 July 2021 •

Published Online: 4 August 2021



View Online



Export Citation



CrossMark

Peter A. Knudsen,<sup>a)</sup>  Kristine Niss,<sup>b)</sup>  and Nicholas P. Bailey<sup>c)</sup> 

## AFFILIATIONS

Glass and Time, IMFUFA, Department of Science and Environment, Roskilde University, P.O. Box 260, Roskilde DK-4000, Denmark

<sup>a)</sup>Electronic mail: [pealkn@ruc.dk](mailto:pealkn@ruc.dk)

<sup>b)</sup>Electronic mail: [kniss@ruc.dk](mailto:kniss@ruc.dk)

<sup>c)</sup>Author to whom correspondence should be addressed: [nbailey@ruc.dk](mailto:nbailey@ruc.dk)

## ABSTRACT

Recent experimental results for the structure in the ionic liquid  $\text{PYR}_{14}^+ \text{TFSI}^-$  have shown invariance in the main structure factor peak along curves of equal electrical conductivity [Hansen *et al.*, Phys. Chem. Chem. Phys. **22**, 14169 (2020)]. The charge peak decreases slightly with increasing temperature at fixed conductivity, however. For simple liquids, curves with invariant dynamics and structure, known as isomorphs, can be identified as configurational adiabats. While liquids with strong-Coulomb interactions do not have good isomorphs, ionic liquids could be an intermediate case with approximate isomorphs along which some aspects of structure and dynamics are invariant. We study a simple molten salt model using molecular dynamics simulations to test this hypothesis. Simple measures of structure and dynamics are investigated along with one transport property, the shear viscosity. We find that there is a substantial degree of invariance of the self-intermediate scattering function, the mean square displacement, and the viscosity along configurational adiabats over a wide range of densities for the three adiabats simulated. The density range studied is more than a factor of two and extends from the strong-Coulomb regime at low densities to the weak-Coulomb regime at high densities. The structure is not invariant over the full range of density, but in the weak-Coulomb regime, we see behavior similar to that seen experimentally over density changes of order 15%. In view of the limited structural invariance but substantial dynamical invariance, we designate the configurational adiabats as *isodyn*es.

Published under an exclusive license by AIP Publishing. <https://doi.org/10.1063/5.0055794>

## I. INTRODUCTION

There is growing interest in using room temperature ionic liquids (ILs), e.g., as electrolytes in lithium batteries to make them more stable and safe to use. This is because ILs can be designed with properties such as low vapor pressure and low flammability, which are desirable for a solvent.<sup>1–3</sup> Modern ionic liquids (from now on, the qualifier “room temperature” is to be understood) are salts that are molten at room temperature, typically combining a large organic cation, such as imidazolium, pyridinium, and pyrrolidinium, with an inorganic anion, such as  $\text{PF}_6$ ,  $\text{BF}_4$ , or  $\text{N}(\text{CF}_3\text{SO}_2)_2$ . The flexibility in the choice of the ions enables the optimization of a range of physical properties providing functionality. This has resulted in great interest in ILs for a range of different applications, including electrochemistry,<sup>4</sup> lubrication,<sup>5</sup> catalysis,<sup>6</sup> bio-preservation,<sup>7</sup> and materials synthesis.<sup>8</sup> As a relatively new class of materials, it is important to

carry out extensive studies in order to gain knowledge about their properties in a wide range of thermodynamic conditions. The properties of interest include (1) structural properties that are important for understanding a material's behavior under different conditions; (2) microscopic dynamics, for example, the self-diffusion coefficient that is related to the conductivity and as such clearly important for battery materials; and (3) transport coefficients such as viscosity, which is relevant generally for technological uses of liquids and also because it correlates with diffusivity.

There is a long history of investigating “classical” molten salts, such as the alkali halides (e.g., NaCl) both theoretically and with simulations, and it has long been understood that in these cases, charge ordering plays an important role, leading to the suppression of concentration fluctuations compared to non-charged mixtures at long wavelengths and effective screening of the Coulomb interactions at long ranges.<sup>9–11</sup> There have also been many attempts in the

literature to understand the dynamics and transport properties of molten salts using the so-called “corresponding states” principle, by which systems can be mapped to a reference system usually involving scaling by the density and temperature of the critical point (or triple point).<sup>12–14</sup>

While measurements at ambient pressure would seem to be sufficient for materials that are intended for applications at that pressure, greater insight can often be obtained by varying pressure as well as temperature. An example of this is the phenomenon of density scaling, whereby dynamical properties are found to be a function not of pressure  $p$  and temperature  $T$  separately or of (number) density ( $\rho$ ) and temperature ( $T$ ) separately but of the combined variable  $\rho^\gamma/T$ , where the density scaling exponent  $\gamma$  is often taken to be a material dependent constant.<sup>15–17</sup> The insight arising from density scaling is twofold: (1) The phase diagram is simpler than otherwise would be considered, being effectively one-dimensional instead of two-dimensional, at fixed composition, and (2) the density (or volume), rather than pressure, is shown to be a more relevant thermodynamic parameter for understanding the structure and dynamics. Density scaling may also be described by saying that one or more dynamical or structural parameters are invariant along curves in the phase diagram, given in the above case by  $T \propto \rho^\gamma$ .

Density scaling has been found to hold for conductivity and/or viscosity of many different ionic liquids.<sup>18–20</sup> Of particular interest for this work are studies on the ionic liquid  $\text{PYR}_{14}^+ \text{TFSI}^-$  [1-butyl-1-methylpyrrolidinium bis(trifluoromethanesulfonyl)imide] where it has been demonstrated that the viscosity, diffusion coefficient, conductivity, and intermediate scattering function studied with inelastic neutron scattering all obey density scaling with  $\gamma = 2.8$ .<sup>21–23</sup> In addition to density scaling of various transport properties and dynamics, it was shown by Hansen *et al.*<sup>23</sup> that the main peak's position and height in the structure factor  $S(q)$  determined by x-ray scattering also followed density scaling with  $\gamma = 2.8$  when analyzed in terms of the dimensionless wavenumber  $\tilde{q} = q\rho^{-1/3}$ . In other words, it was found that the main peak of  $S(q)$  was invariant along the same curves in the phase diagram as the dynamical properties. However, the smaller peak at a lower wavenumber, sometimes referred to as the charge peak, was less invariant, reducing in amplitude and moving toward lower values of  $\tilde{q}$  as temperature increased at constant conductivity. The density change in these experiments was a little over 2%.

The study of invariances of physical quantities along certain curves in the phase diagram is greatly aided by the theoretical framework known informally as isomorph theory. The existence of a curve in the phase diagram along which some quantity, for example, the conductivity, is constant is trivial: For any substance, one can identify invariant curves as contours of conductivity. What is non-trivial is when the contours of one physical quantity coincide with those of another. For certain systems, termed R-simple systems, the contours of many structural and dynamical quantities coincide and these curves are then designated as *isomorphs*. The theory specifies that to see the invariances, it is essential to compare the correctly scaled dimensionless versions of physical quantities, referred to as putting them in “reduced units.” The theory also is quite precise about which physical quantities should be invariant in reduced units.<sup>24</sup>

In the formal development of isomorph theory,<sup>25</sup> isomorphs are defined as curves of constant excess entropy  $S_{ex}(\rho, T) \equiv S(\rho, T) - S_{IG}(\rho, T)$ , the entropy after subtracting the ideal gas

contribution for the same density and temperature. These so-called configurational adiabats can be readily identified in computer simulations, as explained in Sec. II. R-simple systems are understood, as a rule, to be those dominated by van der Waals or metallic bonding.<sup>26</sup> Strongly directional bonding and strong Coulomb interactions<sup>26–28</sup> are known to spoil R-simplicity. Since Coulomb interactions are important in ionic liquids, it is not *a priori* clear that these liquids have good isomorphs. However, the experimental results of Hansen *et al.*<sup>23</sup> suggest that an analysis in terms of isomorphs could be fruitful. Indeed, the coincidence of the invariant main peak in  $S(q)$  and the invariance of conductivity points strongly toward the existence of underlying approximate isomorphs. We say approximate because the charge peak in  $S(q)$  was not observed to be invariant.

A possible interpretation of these results is that the Coulomb interactions play a limited role in determining the structure as given by the main peak of  $S(q)$  and a limited role in determining the dynamical and transport properties. Therefore, approximate isomorphs exist along which these quantities are nearly invariant. On the other hand, the charge peak, which is ascribed to charge ordering and therefore is solely due to the Coulomb interactions, is somehow decoupled from the interactions that determine the main structural and dynamical properties.

In systems that do not have good isomorphs or have at best approximate isomorphs, we can still identify configurational adiabats and investigate structural and dynamical invariances along them. However, it is not appropriate to refer to them as isomorphs. In this work, we will therefore refer to the identified curves as adiabats for correctness (the qualifier “configurational” will always be understood if omitted).

Our goal is to get a better understanding of this behavior—substantial, but not complete invariance of structure and dynamics along the same curves in the phase diagram of an ionic liquid—by studying a simple model system using computer simulations. For this, we have used the simple salt model of Hansen and McDonald,<sup>29</sup> which contains two types of spherical particles differing only in the sign of their charge. This model, described more completely in Sec. III, is designed to be the simplest possible model of an ionic liquid. It consists of point particles interacting via a short-range repulsive inverse power law (IPL) together with Coulomb interactions that are repulsive or attractive for like or unlike particles, respectively. The IPL term by itself would give perfect isomorphs due to the well-known scaling properties of power law functions.<sup>30</sup> The Coulomb interactions, as argued above and in previous work, tend to spoil the pressure–energy correlations that give rise to isomorphs. Inspired by the experimental results, we hypothesize that in this model, there is a similar division into structural [main peak of  $S(q)$ ] and dynamical properties, which are insensitive to the Coulomb interaction, and structural properties [the “charge peak” in  $S(q)$ ], which are sensitive to the Coulomb interaction. We will argue below that because the exponent of the Coulomb interaction ( $n = 1$ ) is much smaller than that of the short-range repulsive IPL ( $n = 9$ ), the charge peak should decrease as density increases along an isomorph (the temperature that would tend to preserve the charge peak is lower than that which preserves the main peak, so the charge peak experiences greater thermal disruption).

Briefly, our main results are that dynamical and transport properties are invariant along configurational adiabats over more or less the full range of densities simulated, while structural properties vary

substantially when the full range of simulated densities is considered. When considering a smaller density range, around a 15% increase, in the high density (weak-Coulomb) regime, the structure appears more invariant; in particular, the main peak in the structure factor, corresponding to the number fluctuations, is quite invariant, while the charge peak, corresponding to concentration fluctuations, varies slightly, in a manner similar to the experiments of Hansen *et al.*,<sup>23</sup> getting smaller and moving toward lower reduced wavenumbers as density increases.

## II. ISOMORPH THEORY

Isomorph theory is a theoretical framework that was first presented in Ref. 24. The theory describes curves in the phase diagram, called isomorphs, along which many structural and dynamical properties are invariant when the quantities of interest are scaled appropriately. Not all systems have isomorphs, and the theory is only exact for systems where the potential energy between particles can be described with an inverse power law,  $V(r) = \epsilon r^{-n}$ . However, this does not mean that it can only describe these systems. For example, in most soft-sphere models, to avoid overlapping particles, the potential energy between particles will monotonically approach infinity as  $r$  goes to 0. This suggests that for small values of  $r$  the potential can be approximated with an inverse power law. This is why we often expect isomorphs at higher densities for these systems. A concrete way to test the “quality” of a potential isomorph through a given state point is by calculating the Pearson correlation coefficient  $R$  between the potential energy and the virial,

$$R = \frac{\langle \Delta W \Delta U \rangle}{\sqrt{\langle (\Delta W)^2 \rangle \langle (\Delta U)^2 \rangle}}, \quad (1)$$

where  $\Delta W$  is the deviation of the virial from its thermodynamic average,  $\Delta U$  is the deviation in potential energy, and  $\langle \dots \rangle$  denotes the canonical (NVT) ensemble average. The  $R$ -value can be calculated for any state point, but a system is usually expected to only have good isomorphs in parts of the phase diagram where  $R > 0.9$ .<sup>24</sup>

In order to trace the isomorph in the phase diagram, one has to calculate another important quantity for isomorphs, the density scaling exponent  $\gamma$ ,

$$\gamma(\rho, T) \equiv \left( \frac{d \ln T}{d \ln \rho} \right)_{S_{ex}} = \frac{\langle \Delta W \Delta U \rangle}{\langle (\Delta U)^2 \rangle}, \quad (2)$$

where  $T$  is the temperature,  $\rho$  is the density, and  $S_{ex}$  is the excess entropy.<sup>24</sup> Thus,  $\gamma$  defined in this way is the slope of the configurational adiabat through a given state point in a double-logarithmic representation of the  $\rho, T$  phase diagram. This is a general statistical mechanical identity; for systems with good isomorphs, the (configurational) adiabats are the isomorphs. Moreover, if  $\gamma$  is independent of density and temperature, then the adiabats have the form  $T \propto \rho^\gamma$ ; this is the case referred to in the Introduction in the context of experimental results on density scaling. In computer simulations, larger changes in  $\rho$  can be explored and  $\gamma$  is generally seen to depend on it and, to a lesser extent, on  $T$ .<sup>31</sup> By treating Eq. (2) as a first order differential equation, we can trace adiabats in the phase diagram via a simple Euler numerical integration,

TABLE I. Table of scaling factors for conversion to reduced units.

Name	Symbol	Reduced symbol	Scaling factor
Distance	$r$	$\tilde{r}$	$\rho^{1/3}$
Inverse distance	$q$	$\tilde{q}$	$\rho^{-1/3}$
Time	$t$	$\tilde{t}$	$\rho^{1/3} \sqrt{k_B T / m}$
Mean square displacement	MSD	MSD (reduced)	$\rho^{2/3}$
Viscosity	$\eta$	$\tilde{\eta}$	$\rho^{-2/3} (mk_B T)^{-1/2}$

$$T_{n+1} = T_n \left( \frac{\rho_{n+1}}{\rho_n} \right)^{\gamma_n}. \quad (3)$$

As mentioned in the beginning, the invariance in structure and dynamics can only be seen when scaled appropriately. These scaling factors are defined for the characteristic properties of the system, such as the density  $\rho$ , the (mean) mass of the particles  $m$ , and the temperature  $T$ . As an example, the scaled distance is  $\tilde{r} \equiv \rho^{1/3} r$ . A list of the reduced units and the necessary scaling factors, which we will use in this paper, can be seen in Table I.

## III. SIMULATIONS

### A. Simple salt model

We have worked with the simple salt model described in Ref. 29. This model contains two types of spherical particles, designated A and B, which are identical except for their opposite charge. The potential contains an inverse power law term with exponent  $n = 9$ , which ensures that all particles are repelled at small distances. It also contains an inverse power law term with exponent 1 that represents the electrostatic interactions between the particles. This means that this term is repulsive for particles of the same type and attractive for particles of different types. The pair potential of this model is thus given by

$$V_{\alpha\beta}(r) = \frac{1}{9} \left( \frac{1}{r} \right)^9 + \epsilon_{\alpha\beta} \left( \frac{1}{r} \right), \quad (4)$$

where  $r$  is the distance between the particles,  $\epsilon_{AA} = \epsilon_{BB} = 1$ , and  $\epsilon_{AB} = \epsilon_{BA} = -1$ . Due to the symmetry of this potential, we will be referring to AA as the like-part and AB as the unlike-part.

Traditionally, in computer simulations, Coulomb interactions have been implemented using some variant of the Ewald-summation method in order to handle the long range part of the interactions as efficiently as possible.<sup>32</sup> It has been shown, however, that for bulk systems a simpler approach, omitting the long range part of the interactions, is sufficiently accurate.<sup>33</sup> In particular, the use of the so-called shifted-force cutoff, whereby a constant term is added to the pair-force such that it vanishes at the cutoff, gives accurate results without requiring excessively large cutoffs.<sup>34,35</sup> This ensures the continuity of the force at the cutoff, giving greater energy stability, although it involves changing the pair potential (by a linear term) at distances less than the cutoff. In this work, we use a shifted-force cutoff for the entire interaction, with a cutoff distance of  $r_c = 6$ . To confirm that this is sufficiently accurate, we have investigated the

effect of systematically reducing the cutoff to 3 at the lowest density of  $\rho = 0.75$  by focusing on the partial structure factors. For the smallest cutoff values, 3 and 4, effects can be seen in the charge-density fluctuations at low wavenumbers (see Fig. 1 of the [supplementary material](#)). There is little change once the cutoff exceeds 5, however. The graph of the potential is shown in Fig. 1. Note that the minimum of the unlike interaction occurs at  $r = 1$ , so naively we expect (Coulomb) attractions to be most relevant at densities below approximately unity (taking the interparticle spacing to be roughly  $\rho^{-1/3}$ ).

At short distances, the purely repulsive  $n = 9$  term dominates so that we expect the Coulomb interaction to play a decreasing role as density increases. In fact, it can be shown mathematically that reducing the contribution of the Coulomb interaction term can be absorbed by a redefinition of length and energy scales or equivalently changing temperature and density to higher values (see Sec. I of the [supplementary material](#)). We therefore simulate a wide range of densities, much wider than would normally be covered in a real experiment on a given material, to probe the effect of effectively reducing the Coulomb interactions. In experiments, one would have to vary the charges, or more likely, vary the size of the molecule while keeping the charges fixed, thus “diluting” their effect.

Hansen and McDonald studied their model at one particular density, 0.3676, and one particular temperature, 0.0177. This density is significantly lower than unity and lower than the densities we study by at least a factor of 2. When converted to real units corresponding to NaCl, the state point is roughly in the vicinity of the experimental triple point of NaCl (20% higher in temperature and 10% lower in density). NaCl is of course a strongly ionic liquid, where the Coulomb interaction very much dominates. In this low density, low temperature regime (compared to the location and depth of the attractive minimum), one expects very weak correlations and no isomorphs. Our interest is inspired by room temperature ionic liquids, on the other hand, in which the Coulomb interactions do not dominate so much, giving an intermediate situation whereby a higher degree of  $W$ ,  $U$ -correlation, and thereby potential for isomorph-like invariances, can be expected. As shown below, the part of the phase diagram we investigate covers values of the correlation coefficient  $R$  ranging from low-to-intermediate ( $R \sim 0.7$ ) to very high ( $R > 0.95$ ). Since the region we simulate is well above the

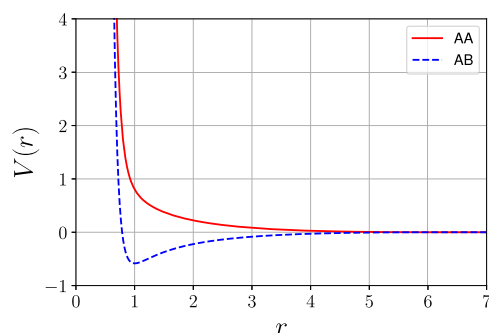


**FIG. 1.** Potential energy between particles in the simple salt model with a shifted-force cutoff implemented at  $r_c = 6$ . Interactions between particles of the same type, AA and BB, are identical. The minimum for the unlike interaction is at  $r = 1$ .

critical temperature and density,<sup>36</sup> one may prefer the term “supercritical fluid” rather than “liquid.”<sup>37</sup> In the context of isomorph theory, this distinction has little physical meaning, however, at least where good isomorphs exist, since one can follow an isomorph from the liquid into the supercritical fluid and observe no essential differences at the microscopic scale; we therefore choose to stick with the term “liquid.”

In the weak-Coulomb regime at high density, we hypothesize that the main effect of Coulombic interactions is to induce a mild degree of charge ordering, while the short-range repulsive term dominates most of the properties, including the slope of the adiabats (that is,  $\gamma$  is close to 3 in this limit). For a pure Coulomb system, the adiabats would have a much lower slope of 1/3; thus, the temperature along the actual adiabats is “too high” for the Coulomb interactions, which is expected to lead to a decrease in charge ordering with increasing density along an adiabat.

## B. Simulation details

We simulated 8000 particles in a rectangular box with sides  $2L \times L \times L$ . The doubled length in the x-direction was chosen to achieve higher resolution in the structure factor.<sup>38</sup> Periodic boundary conditions were implemented to create the perception of a larger system, removing the need to define particle interactions with walls. For simplicity, we chose the masses of both types of atoms to be unity.

The time step was chosen to have a fixed value in reduced units,  $d\tilde{t} = 0.004$ , or  $dt = 0.004\rho^{-1/3}(T/m)^{-1/2}$ . Keeping a fixed value is convenient when comparing dynamical quantities along an isomorph, although it is not essential. For the initial configurations, the particles were placed on an fcc lattice with types assigned randomly. This lattice is not thermodynamically stable and immediately melts at all simulated densities and temperatures. The state points along the isotherms was simulated in parallel (at the same time) since they are independent of each other. Each state point equilibrated for  $2 \cdot 10^6$  time steps before data was collected. The adiabats on the other hand have to be run in series (in order) because the next state point is dependent on the current one [since  $\gamma$  determined in one simulation determines the temperature of the next one via Eq. (3)]. After the initial equilibration, all simulations collected data for  $2^{17} \cdot 100 = 13\,107\,200$  time steps. The simulations were performed using RUMD (Roskilde University Molecular Dynamics),<sup>39</sup> which is designed for a GPU-cluster.

## C. Simulation protocol

Figure 2 shows all simulated points in a  $\rho - T$  phase diagram. We choose three different adiabats to study: one going through the point  $\rho = 0.75$  and  $T = 0.1$ , another going through  $\rho = 1.00$  and  $T = 0.1$ , and finally one through  $\rho = 1.20$  and  $T = 0.1$ . These will be referred to as adiabats 1, 2, and 3, respectively. These three starting densities were chosen such that the forces between unlike particles would be mostly attractive for adiabat 1, neutral for adiabat 2, and repulsive for adiabat 3. This can be seen in Fig. 1 by remembering that the average distance between the particles is given approximately by  $\rho^{-1/3}$ . All three adiabats were simulated from their starting density to  $\rho = 2$ . The results from these adiabats will be compared with six different isotherms  $T = 0.10, 0.15, 0.20, 0.30, 0.50, 1.00$ .

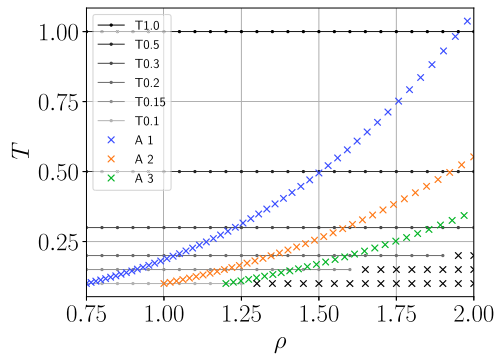


**FIG. 2.** Simulated adiabats and isotherms in a  $\rho - T$  phase diagram. The state points where crystallization was observed are marked with an X.

These temperatures were chosen to overlap with the temperature range of the adiabats. These isotherms were simulated in a density interval from  $\rho = 0.75$  to  $2.0$  with a spacing of  $0.05$ .

At the lowest temperatures and highest densities, crystallization occurred; these points are indicated with a cross in Fig. 2 and omitted from further analysis.

#### IV. RESULTS

Figure 3 shows  $R$  and  $\gamma$  for all adiabats and isotherms plotted as a function of density. For both adiabats and isotherms,  $R$  and  $\gamma$  increase monotonically as the density increases. In the high density limit, they must approach 1 and 3, respectively, since the potential is better approximated by the IPL at high densities at which the isomorph theory is exact and for which  $\gamma$  is given by one third of the exponent  $n = 9$ . In this limit, there are perfect isomorphs and there is no need to simulate; most of our simulated state points (primarily those at lower densities), on the other hand, have  $R < 0.9$ ; thus, we expect less than perfect invariance, with potentially some quantities more invariant than others. The fact that  $\gamma < 3$  in general is not obvious *a priori*; indeed, for the Lennard-Jones potential, which has the same form as the attractive (unlike particles) potential in this model,  $\gamma$  converges to  $12/3 = 4$  from above rather than below. The dependence of  $\gamma$  on density will be discussed below.

##### A. Dynamics and transport

As measures of microscopic dynamics, we consider the mean square displacement (MSD) and self-intermediate scattering function,  $F_s(q, t)$ . The tagged-particle MSD was calculated as an average over particles and time-origins,

$$\text{MSD}(t) = \langle |\mathbf{r}(t) - \mathbf{r}(0)|^2 \rangle, \quad (5)$$

where  $\mathbf{r}(t)$  is the position of a particle at time  $t$ ,  $|\cdot|$  denotes the absolute value, and  $\langle \cdot \rangle$  denotes the ensemble average.

Figure 4(a) shows reduced-unit MSD curves in blue for adiabat 1 and in red for isotherm  $T = 0.1$ . The blue curves collapse perfectly, indicating a strong invariance of this dynamical quantity

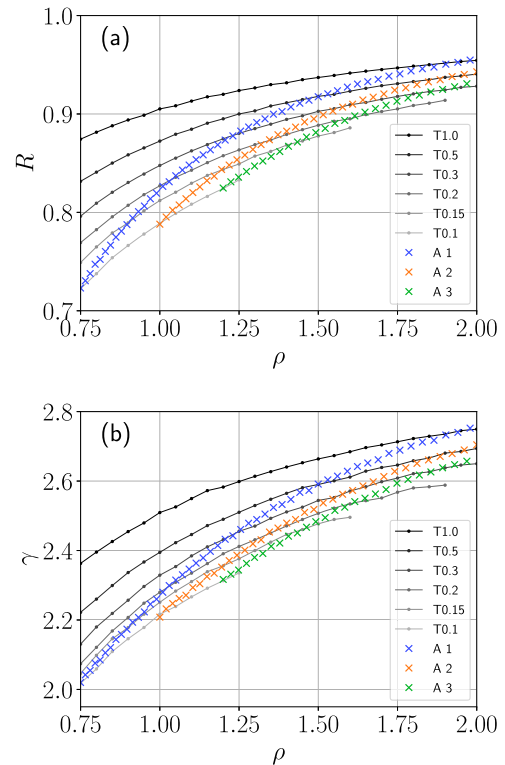


**FIG. 3.** (a) Correlation coefficient  $R$  along adiabats and isotherms as a function of density. (b) Scaling exponent  $\gamma$  along adiabats and isotherms as a function of density.

along configurational adiabats. The curves show the usual transition from a ballistic regime at short times (slope 2 in a double-log plot) to a diffusive regime (slope 1) at long times. The absence of a plateau between these two regimes is characteristic of non-viscous behavior. This is consistent with the relatively easy crystallization we observe when the high density/low temperature region of the phase diagram is simulated (the crosses in the lower right corner in Fig. 2): The latter indicates that this model cannot be readily supercooled, which implies that we should not expect to find any viscous liquid states. Because the MSD in the ballistic regime depends on temperature and particle mass but not on the potential, it is straightforward to show that it is always equal to  $3t^2$ , and therefore, all data must collapse trivially in that regime. The collapse of the diffusive regime along the adiabat, on the other hand, is a non-trivial result. To show data from all simulations in a concise way, we determine the diffusion coefficient from a linear fit to the MSD data, shown in Fig. 4(b) for all state points. The dynamical invariance along configurational adiabats is manifested over the whole density range on each adiabat.

The self-intermediate scattering function was calculated by

$$F_s(\mathbf{q}, t) = \langle \exp[i\mathbf{q} \cdot (\mathbf{r}(t) - \mathbf{r}(0))] \rangle, \quad (6)$$

where  $\mathbf{r}(t)$  is the position of a particle at time  $t$ .<sup>40</sup> Figure 5(a) shows the intermediate scattering function, plotted as a function of reduced

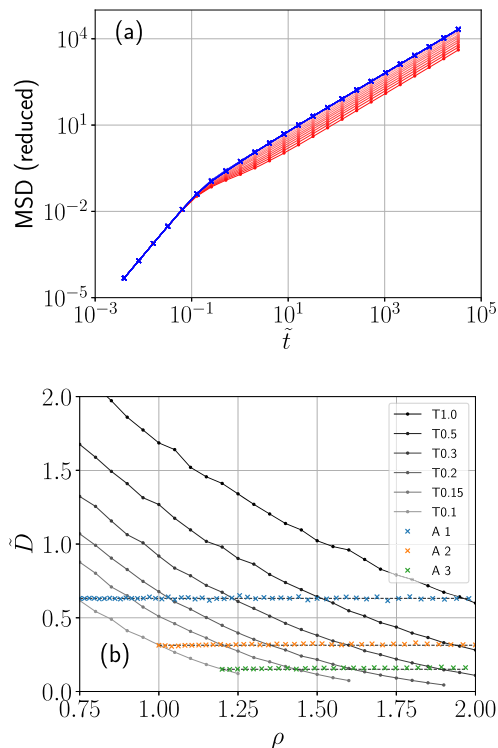


**FIG. 4.** (a) Reduced MSD as a function of reduced time for all densities where crystallization did not occur on isotherm  $T = 0.1$  (red curves) and all state points along adiabat 1 (blue curves). The blue curves collapse on each other. (b) Diffusion coefficient (determined from the long time slope of the MSD) for all adiabats and isotherms. The horizontal dashed lines at the three adiabats are to guide the eye. They pass through the first (lowest density) point of each adiabat.

time  $\tilde{t}$ , for adiabat 1 (blue) and isotherm  $T = 0.1$  (red). The  $q$ -value was chosen to be  $7.1\rho^{1/3}$ , ensuring that it is fixed in reduced units and close to the maximum of  $S_{NN}$  (see Sec. IV B). At all the investigated state points, a simple, near-exponential decay is observed, corresponding to ordinary non-viscous liquid dynamics, and consistent with the absence of a plateau in the MSD data. The red curves in Fig. 5(a) move toward longer times (slower dynamics) as the density increases, while the blue curves collapse on each other, showing that also this measure of dynamics is invariant along adiabat 1. The data for other isotherms and adiabats behave similarly (see Figs. 2–6 of the supplementary material). In Fig. 5(b), we plot the reduced time at which  $F_s$  has fallen to  $e^{-1}$ , denoted as  $\tilde{t}_{1/e}$ , as a function of density for all adiabats and isotherms. This time scale increases rapidly with increasing density at fixed temperature but increases only slightly along adiabats, again indicating rather invariant dynamics. This plot shows that the invariance is not perfect [the slight deviation is hidden in panel (a) of Fig. 5 due to the logarithmic axis] but nevertheless impressive given the large density changes involved. Note that the change in a real time scale over this range of densities is about a factor of 4.5 for adiabat 1. The collapse of the  $F_s$  curves themselves means that the invariance applies to the whole time-dependent relaxation curve, not just the characteristic time scale. Indeed, the shape-parameter  $\beta$  in the stretched-exponential fits

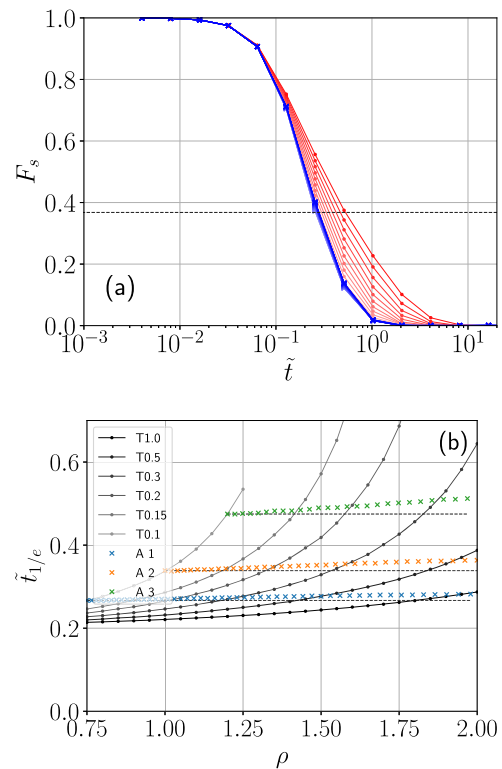


**FIG. 5.** (a)  $F_s$  plotted as a function of reduced time for all simulated densities at  $T = 0.1$  (red curves) and all simulated state points on adiabat 1 (blue curves). The latter collapse almost perfectly on each other. The horizontal dashed line indicates the value  $1/e \approx 0.368$ . (b) Reduced time at which  $F_s = 1/e$ , for all adiabats and isotherms. The horizontal dashed lines pass through the first points (lowest density) of the adiabats and are intended to guide the eye.

is more invariant than the characteristic time except at low densities (left panel of Fig. 9 of the supplementary material). It should be emphasized that the approximate invariance shown by the reduced self-intermediate scattering function applies over the whole simulated range of density, even though the  $W$ ,  $U$ -correlation coefficient  $R$  is less than 0.9 for most of the density range of each adiabat, and as such, we do not expect the configurational adiabats to be isomorphs. Note that at smaller wavenumbers the time scale for the intermediate scattering function becomes more invariant (see Fig. 7 of the supplementary material), consistent with the excellent collapse of the diffusivity data, since diffusion is a long wavelength process.

Finally, in this section, we investigate the viscosity as an important example of a macroscopic transport coefficient. The viscosity was calculated using the Green–Kubo formula,<sup>32</sup>

$$\eta = \frac{V}{k_B T} \int_0^\infty \langle \sigma_{xy}(0) \sigma_{xy}(t) \rangle dt, \quad (7)$$

where  $V$  is the volume of the simulation box,  $k_B$  is the Boltzmann constant,  $T$  is the temperature, and  $\sigma_{xy}(t)$  is the  $xy$  component of the stress tensor as a function of time  $t$ . The calculation of the integral in Eq. (7) is done analytically after fitting the normalized

autocorrelation function at short (reduced) times ( $\tilde{t} \leq 0.06$ ) to a polynomial  $a_0 + a_2\tilde{t}^2 + a_3\tilde{t}^3$  (note that the slope must be zero at  $\tilde{t} = 0$ ) and at longer (reduced) times ( $\tilde{t} \geq 0.06$ ) to a sum of two exponential functions. The data up to where the normalized function first goes below 0.001 are included in the fit. Figure 6(a) shows four examples of the normalized stress autocorrelation function and the corresponding fits. The plot is in reduced units; the two curves from the same adiabat are somewhat similar but not identical when plotted this way. Figure 6(b) shows the reduced viscosity as a function of density along the isotherms and adiabats. As with the self-intermediate scattering function and the mean squared displacement, we find a striking invariance across the whole range of densities for each of the three adiabats. Given that the two curves in Fig. 6(a) from the same adiabat differ at long times, giving different values for the integral of the normalized correlation function, it is surprising that viscosity seems so invariant. The formula for  $\tilde{\eta}$  can be written as the product of the reduced infinite frequency shear modulus  $\tilde{G}_\infty$  and the integral of the normalized shear stress autocorrelation function with respect to reduced time. Figure 10 of the supplementary material shows  $\tilde{G}_\infty$ , which is not invariant but rises noticeably with density along adiabats. This increase compensates for the decrease in the integral of the normalized correlation function, yielding a rather invariant reduced viscosity.

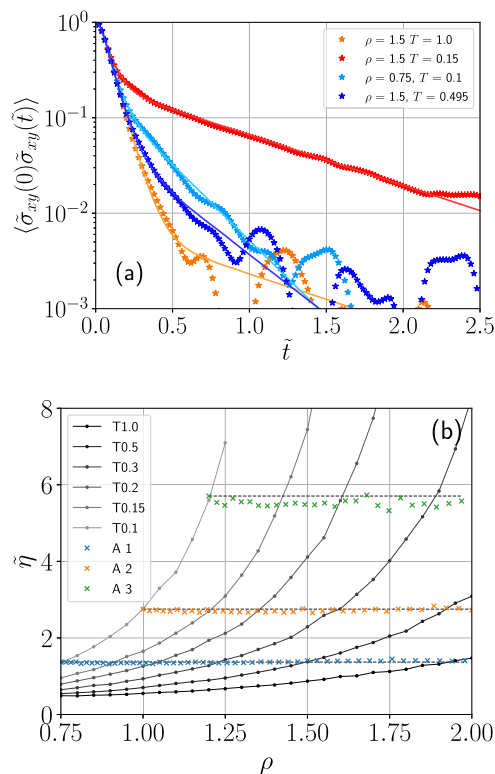


**FIG. 6.** (a) Examples of the normalized stress autocorrelation data and double-exponential fit. The plot is in reduced units to facilitate the comparison of data from the same adiabat. (b) Comparison of the viscosity along adiabats and isotherms. The horizontal dashed lines at the three adiabats are to guide the eye. They pass through the first point of each adiabat.

## B. Structure

To study the structure, we consider both the radial distribution function and the structure factor. We consider partial pair correlation or radial distribution functions  $g_{\alpha\beta}(r)$  defined in the usual way, where the indices  $\alpha$  and  $\beta$  refer to particle types A and B. Only two of these, the AA and AB functions, are independent since the AA and BB interactions are identical and the composition is equimolar. The corresponding partial structure factors  $S_{\alpha\beta}(q)$ , known as the Faber–Ziman (FZ) structure factors, can be defined by Fourier transforming these, but we choose a different representation known as the Bhatia–Thornton (BT) partial structure factors (see Fig. 16 of the supplementary material for some FZ structure factor data). These are defined for binary mixtures<sup>38,41</sup> as certain linear combinations of the FZ structure factors, denoted as NN, NC, and CC, where N refers to number density fluctuations and C refers to concentration density fluctuations. Section II of the supplementary material explains how this representation is equivalent to defining sum and difference variables of the Fourier components of density fluctuations.<sup>9</sup> If  $c_A$  and  $c_B$  are the concentrations of species A and B, respectively, then the BT partial structure factors are defined by<sup>38,41</sup>

$$S_{NN}(q) = c_A^2 S_{AA}(q) + c_B^2 S_{BB}(q) + 2c_A c_B S_{AB}(q) > 0, \quad (8)$$

$$S_{CC}(q) = c_A c_B [1 + c_A c_B (S_{AA}(q) + S_{BB}(q) - 2S_{AB}(q))] > 0, \quad (9)$$

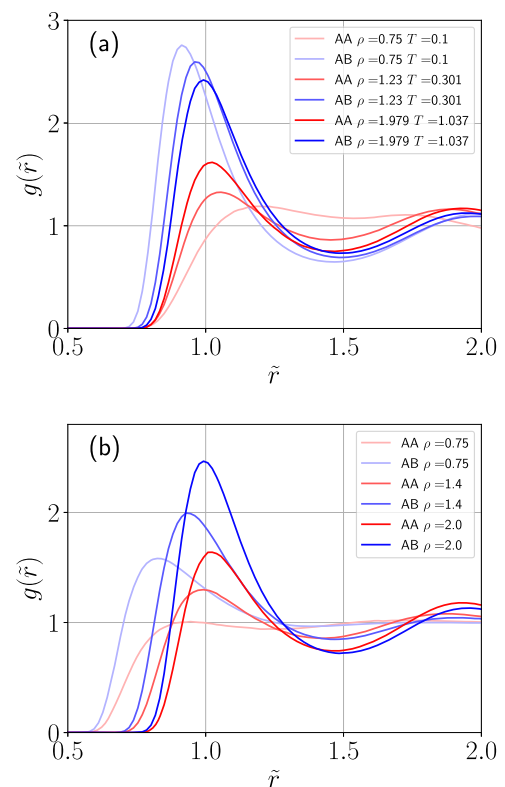


**FIG. 7.** Partial radial distribution functions for three state points on (a) adiabat 1 and (b) isotherm  $T = 1.0$ , plotted as functions of reduced distance  $\tilde{r}$ .

$$S_{NC}(q) = c_A c_B [c_A (S_{AA}(q) - S_{AB}(q)) - c_B (S_{BB}(q) - S_{AB}(q))]. \quad (10)$$

In our system,  $S_{AA}(q) = S_{BB}(q)$  and  $c_A = c_B = 0.5$ , and thus  $S_{NC} = 0$ , and we do not include it in our analysis. The utility of this representation stems from the way in which the coherent part of the total neutron scattering signal is written<sup>38</sup> (taking  $S_{NC} = 0$ ),

$$\frac{1}{N} \left[ \frac{d\sigma}{d\Omega}(q) \right]^{\text{coh}} = |\langle b \rangle|^2 S_{NN}(q) + |\bar{b}_A - \bar{b}_B|^2 S_{CC}(q), \quad (11)$$

where  $\bar{b}_\alpha$  is the spin- and isotope-averaged scattering length for species  $\alpha$  and the angle brackets denote averaging over different species. For x-ray scattering, the scattering lengths should include an additional  $q$ -dependence from the atomic form factor, while the spin-averages can be dropped (the total cross section will also include other effects<sup>38</sup>). Thus, the NN part of the structure factor is coupled to the mean scattering length and thus is what would be measured by a probe insensitive to chemical species. Fischer refers to it as the “colour-blind” scattering cross section.<sup>38</sup> The CC part is measured only when the scattering length differs between chemical species and describes chemical ordering. For our ionic system, we can associate the charge peak in the total scattering signal with a peak in  $S_{CC}(q)$ . As mentioned, one can obtain the BT partial structure factors by appropriately Fourier transforming the partial pair correlations to get the FZ structure factors. To avoid truncation

of the Fourier transform, we used instead the more rigorous method of saving Fourier components of the density fluctuations for each species at regular intervals and then taking the relevant (co-)variances before taking appropriate linear combinations to form the BT partial structure factors (Sec. II of the [supplementary material](#)). When calculating  $S(q)$  this way, only Fourier modes that fit into the simulation box are allowed. We take the first 88 modes in the  $x$ -direction, which gives sufficient resolution to resolve the peaks. By considering modes that fit into the box, we have different  $q$ -values at different densities, but the reduced-unit wavenumbers  $\tilde{q} \equiv \rho^{-1/3} q$  are identical, which is necessary for isomorph-compatible comparison. Note that  $S_{CC}(q)$  tends toward the product of concentrations  $c_A c_B = 1/4$  in the limit of zero chemical ordering.

[Figure 7](#) shows the partial radial distribution functions for selected densities on adiabat 1 and isotherm  $T = 1.0$ , while [Fig. 8](#) shows the BT partial structure factors on the same state points. Reduced units  $\tilde{r}$  and  $\tilde{q}$  have been used in the plots for both quantities. There is substantial variation in both structural measures as the density varies, confirming that the adiabats we have simulated are not isomorphs despite the fact that dynamical quantities are remarkably invariant along them. The most that can be said is that the structural measures vary less with density on adiabats than on isotherms. A general feature for all adiabats and isotherms is that the features in both  $g_{AA}(\tilde{r})$  and  $S_{NN}(\tilde{q})$  become more pronounced as the density increases. Furthermore, as density increases along the

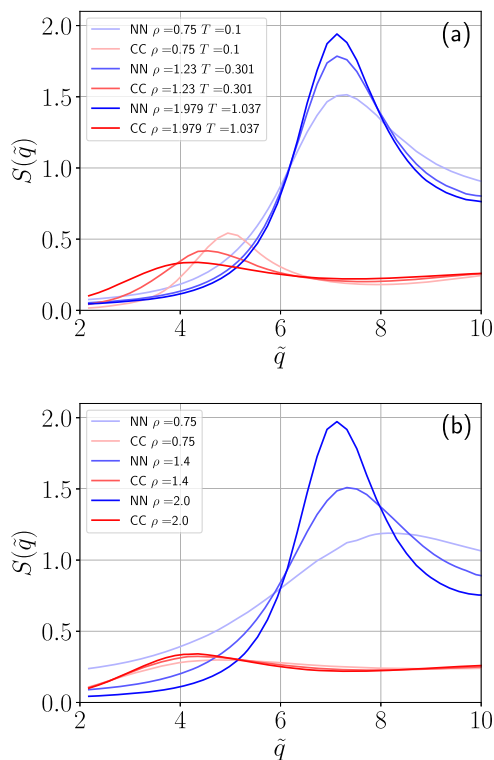


**FIG. 8.** Bhatia–Thornton structure factors for three state points on (a) adiabat 1 and (b) isotherm  $T = 1.0$ , plotted as functions of reduced wavenumber  $\tilde{q}$ .

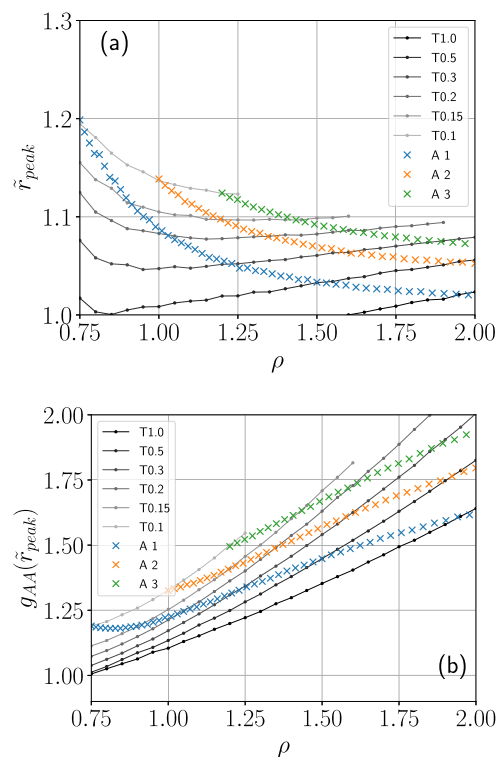


**FIG. 9.** Dependence of (a) the reduced-unit position and (b) the height for the first peak of the AA partial radial distribution function on density for all six isotherms and all three adiabats.

adiabats, the first peak in  $S_{CC}(\vec{q})$  moves to lower  $\vec{q}$ -values and the peak height decreases. Recalling that the CC peak can be identified with the charge peak, this is the same behavior as seen in Ref. 23, and it is not shared with the isotherms. Indeed, Fig. 8(b) shows that the peak in  $S_{CC}(q)$  is actually rather invariant along the isotherm; its height and position depend mainly on temperature alone.

Recall that we expect more isomorph-like behavior, that is, better invariance, in the limit of high density. To investigate how this occurs, and to get a more simple view of how the structure changes along the adiabats and isotherms, we have analyzed the position and height of the first peaks in  $g(\vec{r})$  and  $S(\vec{q})$ . This was done by fitting a fourth order polynomial to data around the peak. Focusing on the peak position and height makes it easier to analyze trends in the data across the whole range of densities. Considering the radial distribution function first peaks, Figs. 9 and 10, both the peak position and peak height vary significantly along adiabats, but it is also clear that they are beginning to level off at the highest densities, whereas the data for isotherms give no indication of leveling. The leveling off for the adiabats is clearer for the peak positions than for the peak heights, although we note that for  $g_{AA}(r)$  the overall variation in the peak position is greater for adiabats than for isotherms, which exhibit a shallow minimum at low densities. Another feature of the adiabats is that the AA peak position starts at values around 1.15 and decreases to values around 1.05, while the AB peak position starts at values below unity and increases to values just above unity. Thus,

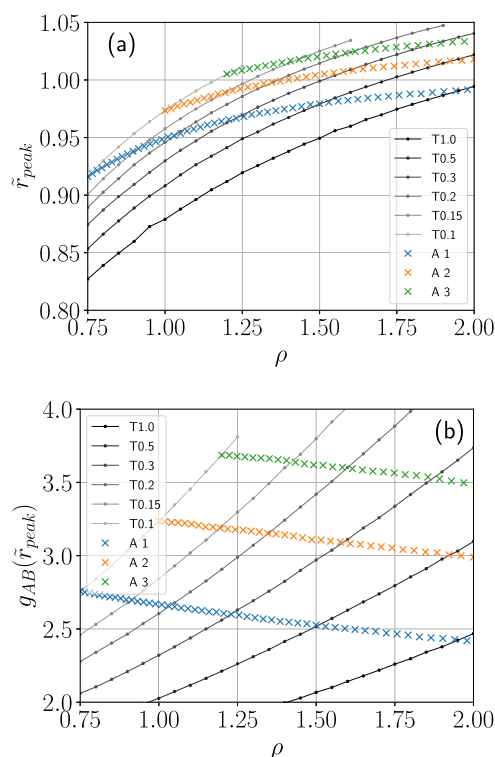


**FIG. 10.** Dependence of (a) the reduced-unit position and (b) the height for the first peak of the AB partial radial distribution function on density for all six isotherms and all three adiabats.

for each adiabat, both peaks start significantly separated, by about 20%–30%, and converge with increasing density, being separated by only a few percent at the highest densities shown. This convergence is consistent with the hypothesis that charge ordering, and hence particle identity, becomes less important as the density increases.

While both peak heights increase with density on isotherms, which is expected, they move oppositely along adiabats, increasing sharply for AA from low values and decreasing gently for AB from high values. That is, they move toward each other, again reflecting the tendency for AA and AB structures to become more alike as charge ordering diminishes along adiabats.

We turn next to the peak analysis of the BT partial structure factors,  $S_{NN}(\vec{q})$  (Fig. 11) and  $S_{CC}(\vec{q})$  (Fig. 12). The leveling out observed in the radial distribution functions is more pronounced in the NN peak heights and positions, whereas it is less pronounced in the CC plots. Over the last 0.5 or so of density, the relative change in the NN peak heights is small, while the relative change in the CC peak heights is substantial. It must be noted, however, that the absolute value of the CC peak is initially quite small, and therefore, the absolute changes in NN and CC peak heights are rather comparable. Recall that we expect that at sufficiently high density the Coulomb interactions become irrelevant, and therefore, charge ordering will be negligible; as mentioned above,  $S_{CC}(q)$  should tend toward  $c_{ACB} = 0.25$ , which is consistent with the observed behavior; the variation in the CC peak height is the already rather small degree of

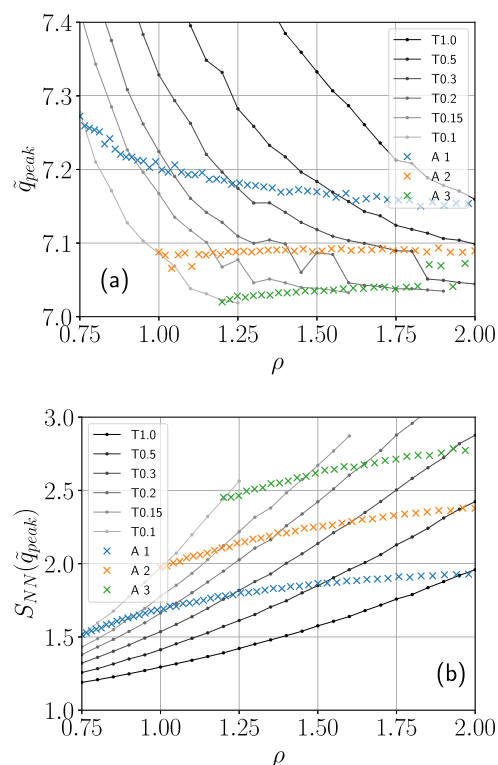


**FIG. 11.** Dependence of (a) the (reduced-unit) position and (b) the height for the first peak of the NN Bhatia-Thornton partial structure factor on density for all six isotherms and all three adiabats.

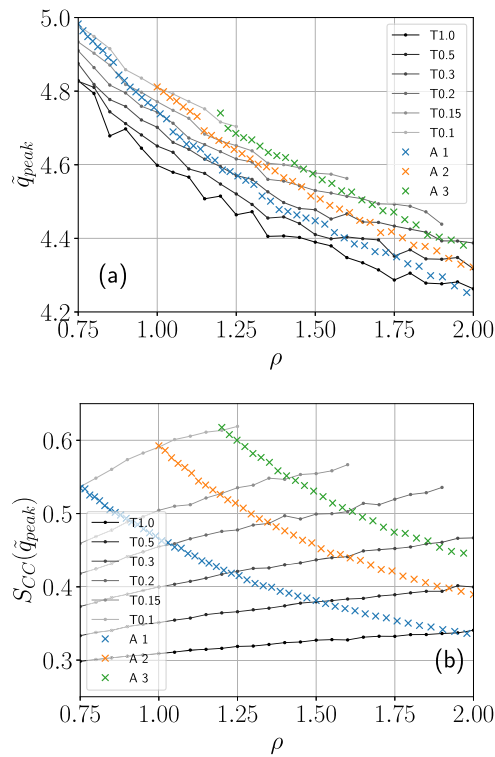


**FIG. 12.** Dependence of (a) the (reduced-unit) position and (b) the height for the first peak of the CC Bhatia–Thornton partial structure factor on density for all six isotherms and all three adiabats.

charge ordering getting even smaller. To illustrate the high density behavior more directly, we show a collapse of both Bhatia–Thornton structure factors for adiabat 2 over the density range of 1.75–2.00 in Fig. 13 and a density increase of 14%. Similar plots can be made

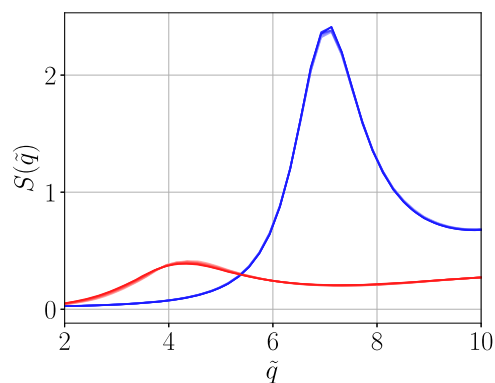


**FIG. 13.** NN (blue) and CC (red) Bhatia–Thornton partial structure factors for adiabat 2, including densities from 1.75 to 2.0. There are seven red curves and seven blue curves, with the intensity of the lines increasing with increasing density. The NN curves increase slightly but systematically in peak height with increasing density, while a slight but systematic decrease of both the CC peak height and CC peak position is noticeable.

for the other adiabats and also over the density range of 1.5–1.75 (Figs. 13–15 of the [supplementary material](#)). The most important point here is that the structure is in fact rather invariant over this density range, comparable to what is seen with good isomorphs (indeed, this density range is larger than that investigated in the first isomorph paper<sup>24</sup>). Second, the visible deviations are very small and confined to very top of the peak for NN, while they are more spread out for CC, related to the fact that the CC peak varies in position as well as height.

A more concrete way to analyze charge ordering is to determine the partial coordination numbers, i.e., the numbers of near-neighbors of each type that a given particle has. The data for these are presented and discussed in the [supplementary material](#) (Figs. 11 and 12 of the [supplementary material](#)) and consistent with the other structural analyses, in that the total coordination number is rather invariant on adiabats, while the concentration of like particles in the neighbor shell increases toward presumably 50%, as the particle identity becomes less relevant.

## V. DISCUSSION

### A. Density dependence of the density scaling exponent

The value of the density scaling exponent  $\gamma$  and how it depends on density are interesting not least because it can be directly compared with experiment. Indeed, the values we observe here are in the range (2–3.5) considered typical for ionic liquids. For R-simple systems consisting of spherical particles interacting with pairwise forces,  $\gamma$  can be straightforwardly related to derivatives of the potential,<sup>42</sup> but in other systems the connection to the potential is not so straightforward. For the present system, it turns out that the value and density dependence of  $\gamma$  can be essentially explained by a single approximation, namely, that fluctuations of the Coulomb contribution to the energy are uncorrelated with those of the IPL contribution. Some data justifying this assumption are given in the [supplementary material](#) (Fig. 19 of the [supplementary material](#)). Specifically, if we write a fluctuation of potential energy as a sum of two terms,

$$\Delta U = \Delta U_{IPL} + \Delta U_C, \quad (12)$$

then the corresponding fluctuation in the virial is

$$\Delta W = \Delta W_{IPL} + \Delta W_C = 3\Delta U_{IPL} + (1/3)\Delta U_C, \quad (13)$$

where we used the fact that each term separately is an IPL and therefore exhibits perfect  $W, U$  correlations with a coefficient given by one third of the IPL exponent. Putting this into the expression for  $\gamma$ , Eq. (2) gives

$$\gamma = \frac{3\langle(\Delta U_{IPL})^2\rangle + 3\frac{1}{3}\langle\Delta U_{IPL}\Delta U_C\rangle + \frac{1}{3}\langle(\Delta U_C)^2\rangle}{\langle(\Delta U_{IPL})^2\rangle + 2\langle\Delta U_{IPL}\Delta U_C\rangle + \langle(\Delta U_C)^2\rangle}. \quad (14)$$

Making the assumption  $\langle\Delta U_{IPL}\Delta U_C\rangle = 0$ , i.e., uncorrelated contributions from the IPL and Coulomb terms, leads to a simpler expression,

$$\gamma = \frac{3 + X/3}{1 + X}, \quad (15)$$

where  $X \equiv \langle (\Delta U_C)^2 \rangle / \langle (\Delta U_{IPL})^2 \rangle$  is the ratio of variance of Coulomb energy fluctuations to that of IPL energy fluctuations. In the limit of high density, this ratio is expected to vanish, giving  $\gamma \rightarrow 3$ ; at lower densities,  $\gamma$  is less than 3. Indeed,  $\gamma$  rises monotonically from 1/3 at high values of  $X$  to 3 as  $X$  vanishes. Thus, the weak correlation between fluctuations of the energy from the Coulomb term and that from the  $n = 9$  IPL explains both the reduction in  $\gamma$  and its increase with increasing density.

### B. Curves of invariant dynamics: *Isodynes*

This model is interesting because simply by varying the density, it covers the range from asymptotically perfect isomorphs at high density down to strongly ionic behavior with no isomorphs at low density. One would expect *a priori* to see the approximate invariance of both structural and dynamical properties in the high density, weak-Coulomb regime, but no particular invariance at low densities (strong-Coulomb regime). This is indeed how it appears when we consider the structure. However, intriguingly, the dynamical quantities we have investigated and the viscosity appear to be nearly invariant on configurational adiabats throughout this density range when expressed in reduced units. In particular, the reduced diffusivity and viscosity show little to no variation along the three adiabats, while the time scale extracted from the self-intermediate scattering function rises slightly, showing a 10% increase in reduced units, e.g., for adiabat 3 over the density range of 1.2–2.0 [Fig. 5(b)]. It is worth pointing out that while the reduced-unit viscosity is invariant, the real viscosity changes by a substantial factor: From Table 1, the real viscosity must be proportional to  $\rho^{2/3} T^{1/2}$ , giving a factor of over 6 increase for the real viscosity along adiabat 1. This invariance of a transport coefficient is consistent with Rosenfeld's excess entropy scaling,<sup>43</sup> but it must be noted that the invariance of also the time-dependent correlation functions is a stronger result than excess entropy scaling alone implies.<sup>44</sup> This discovery for the ionic liquids is a strong effect, which suggests a fundamental perhaps fairly basic origin, although we are not yet in a position to clarify what that origin is. Investigation of different N-body structural contributions to the excess entropy could be fruitful, however. Formally,  $S_{ex}$  can be written as a sum  $S_2 + S_3 + S_4 + \dots$ , where the two-body term  $S_2$  can be determined from the RDF; Dzugutov argued that it is the most important contribution.<sup>45</sup> A natural line of further research would therefore be to investigate its invariance in this system and others where the variation of structure coexists with dynamical invariance.

It is considered a paradigm in materials science that a material's structure determines its properties. Therefore, it is striking to find an example where it does not—for this model, the structure can vary substantially along an adiabat, but the dynamical properties vary hardly at all. This would place the current model system in a wider class of materials than the so-called Roskilde systems (those with good isomorphs). Similar results have been seen in Gnan *et al.*<sup>46</sup> where a colloidal model was studied; they found lines of invariant dynamics (termed *isodynamics lines*) in the  $\phi - T$  phase diagram, but structural and thermodynamic properties were not invariant along these lines. In that work, the isodynamic lines were identified

empirically, as contours of reduced diffusivity, and it was not investigated whether they correspond to configurational adiabats. Nevertheless, their results suggest that the model colloidal system of that work also belongs in the same class of materials as our model. As a third example, recent unpublished simulations of a similar model to the present one<sup>47</sup> but using exponents 8 and 4 rather than 9 and 1 show very similar behavior<sup>48</sup> to the present model. To denote adiabats having the property of approximate dynamical invariance, we could use “isodynamics lines,” following the work of Gnan *et al.*, but we wish to propose the more compact term *isodynes*.

### C. Comparison to experiment

The model studied in this work is far from a realistic model of an ionic liquid. Nevertheless, we find a number of striking similarities in the phenomenology of the model and the measured data. First of all, the model has lines in the phase diagram along which all the studied dynamical and transport properties are invariant. This corresponds to finding density scaling with the same exponent  $\gamma$  for all the dynamical properties as is seen in experiment.<sup>21,23</sup> In the simulations, the value for  $\gamma$  changes with density, which is related to the much larger density range explored.<sup>49</sup> The value found for  $\gamma$  in the model lies in the range of 2–2.8. These values are also typical for experimental ionic liquids where  $\gamma$  is in the range of 2–3.5.<sup>18–21,23</sup> As explained above, the maximum value of  $\gamma$  in the model is 3, which stems from the choice of an  $n = 9$  inverse power law, while it is the Coulomb interactions that make  $\gamma$  decrease below this value. Thus, the Coulomb interactions explain why the density scaling exponents of ionic liquids are typically smaller than the density scaling exponents of van der Waals bonded liquids. However, the numerical agreement between  $\gamma$  of the model and the experimental data should not be overemphasized as it stems from the choice of the power  $n = 9$  in the model.

In addition to density scaling being obeyed by a range of dynamical properties, the structural behavior of the model shows some similarity with the x-ray scattering data in Ref. 23. The relatively large experimental charge peak must reflect a much larger degree of charge ordering that we see in our model (and not, for example, an effect of the mean scattering length being much smaller than its difference between species, which could be possible for neutron scattering). Nevertheless, the changes seen are reasonably consistent with what we observe—the main structure factor peak (the NN partial structure factor) is invariant along lines of constant dynamics for moderate density changes. In the model, the charge peak (the CC partial structure factor) is also quite invariant for a moderate change in density, while it decreases in intensity and moves to lower values of  $\tilde{q}$  with increasing temperature in the experimental results. For larger density changes, this behavior is also seen for the prepeak of the model, while the main peak increases in amplitude [see Fig. 8(a)]. In other words, the structural behavior of the model and the experimental results is not exactly the same, but the tendencies are very similar, and the surprising conclusion that the charge ordering does not affect the dynamics holds in both cases. Indeed, the results from the model suggest the following interpretation of the experimental results: The nearly invariant main peak indicates near-isomorphic behavior when charge ordering is ignored, and this corresponds to invariant dynamics. At the same time, what charge ordering there is decreases as the density

increases along the curve of invariant dynamics. One can conclude that the charge ordering plays no role in the dynamics. Considering the model, since our main peaks increase slightly with increasing density along adiabats, a slightly higher-temperature curve could be found along which the main peak height is constant. Along such a curve, the charge peak would decrease even more noticeably, and the structure would match the experimental data even more. However, presumably, the dynamics would be slightly less invariant, particularly the diffusivity, which is the most invariant quantity we have investigated.

#### D. Comparison with corresponding states approaches

A brief comparison between the present isomorph-based approach and traditional corresponding states approaches<sup>12–14</sup> is appropriate. What the approaches have in common is scaling of the quantities of interest to a dimensionless form for comparison with a reference system or state point. However, in corresponding states, this scaling involves microscopic energy and length parameters associated with the pair potential, while in isomorph theory, it is the density and temperature that are used. Another important difference is that corresponding states approaches identify the critical point (or, sometimes, the triple point) as a key state point by which other state points can be scaled (density and temperature), while in isomorph theory, the excess entropy is the key quantity controlling structure and dynamics (but not the pressure, i.e., the equation of state).  $S_{ex}$  also plays a natural role in comparing different systems (the quasiuniversality principle<sup>50</sup>).

#### VI. CONCLUSION

In our investigation of the model originally proposed by Hansen and McDonald, we have studied higher densities than they did in order to probe the moderate-to-weak Coulomb regime as opposed to the strong-Coulomb regime at low density. We have found evidence of what we call isodynes or isodynamics lines. These are curves of constant excess entropy along which dynamical quantities are remarkably invariant along a wide range of densities, while structural features change noticeably over the same range. On the other hand, restricting to smaller density ranges near the high density (weak-Coulomb) end gives a reasonable degree of isomorph invariance also in the structure, with the main changes visible being the steady reduction of the already small charge ordering. These results are qualitatively in agreement with experimental studies of a room temperature ionic liquid.<sup>23</sup> Possible future work with this model could involve continuing the investigations to lower density, as low as the density studied by Hansen and McDonald,<sup>29</sup> well into the strong-Coulomb regime, in order to see whether the invariance of dynamical quantities persists also there. An initial effort in this direction is presented in the [supplementary material](#) where adiabat 1 has been extended down to a density of 0.3 (Figs. 17 and 18 of the [supplementary material](#)). The dynamical invariances continue, while the structure continues to undergo a significant change (data not shown). Below density around 0.5, shallow minima or maxima appear in the dynamical quantities, but these are very small changes. In addition, realistic models of ILs should be studied to determine whether isodynes can also be identified more generally in these systems.

#### SUPPLEMENTARY MATERIAL

The [supplementary material](#) contains some explanatory text on charge/density scaling and the Bhatia–Thornton structure factors, as well as additional figures and accompanying text as mentioned in the main text.

#### ACKNOWLEDGMENTS

Funding from the Danish Ministry of Higher Education and Science through the ESS SMART Lighthouse is gratefully acknowledged.

#### DATA AVAILABILITY

The data that support the findings of this study are available from the corresponding author upon reasonable request.

#### REFERENCES

- 1 E. W. Castner, Jr. and J. F. Wishart, “Spotlight on ionic liquids,” *J. Chem. Phys.* **132**(12), 120901 (2010).
- 2 J. Dupont, “From molten salts to ionic liquids: A ‘nano’ journey,” *Acc. Chem. Res.* **44**(11), 1223–1231 (2011).
- 3 L. Aguilera, J. Völkner, A. Labrador, and A. Matic, “The effect of lithium salt doping on the nanostructure of ionic liquids,” *Phys. Chem. Chem. Phys.* **17**, 27082–27087 (2015).
- 4 A. Matic and B. Scrosati, “Ionic liquids for energy applications,” *MRS Bull.* **38**(7), 533–537 (2013).
- 5 C. Ye, W. Liu, Y. Chen, and L. Yu, “Room-temperature ionic liquids: A novel versatile lubricant,” *Chem. Commun.* **21**, 2244–2245 (2001).
- 6 H. Olivier-Bourbigou, L. Magna, and D. Morvan, “Ionic liquids and catalysis: Recent progress from knowledge to applications,” *Appl. Catal., A* **373**(1–2), 1–56 (2010).
- 7 K. Fujita, D. R. MacFarlane, and M. Forsyth, “Protein solubilising and stabilising ionic liquids,” *Chem. Commun.* **38**, 4804–4806 (2005).
- 8 D. S. Wragg, G. M. Fullerton, P. J. Byrne, A. M. Z. Slawin, J. E. Warren, S. J. Teat, and R. E. Morris, “Solvothermal aluminophosphate zeotype synthesis with ionic liquid precursors,” *Dalton Trans.* **40**(18), 4926–4932 (2011).
- 9 M. Rovere and M. P. Tosi, “Structure and dynamics of molten-salts,” *Rep. Prog. Phys.* **49**(9), 1001–1081 (1986).
- 10 M. P. Tosi, D. L. Price, and M.-L. Saboungi, “Ordering in metal halide melts,” *Annu. Rev. Phys. Chem.* **44**, 173–211 (1993).
- 11 J.-P. Hansen and I. R. McDonald, *Theory of Simple Liquids with Applications to Soft Matter*, 4th ed. (Academic Press, 2013).
- 12 M. Harada, M. Tanigaki, and Y. Tada, “Law of corresponding states of uni-univalent molten salts,” *Ind. Eng. Chem. Fundam.* **22**, 116–121 (1983).
- 13 Y. Nagasaka and A. Nagashima, “Corresponding states correlation for the thermal conductivity of molten alkali halides,” *Int. J. Thermophys.* **14**, 923–936 (1993).
- 14 N. Galamba, C. A. Nieto de Castro, I. Marrucho, and J. Ely, “A corresponding-states approach for the calculation of the transport properties of uni-univalent molten salts,” *High Temp. - High Pressures* **33**, 397–404 (2001).
- 15 A. Tölle, H. Schober, J. Wuttke, O. G. Randl, and F. Fujara, “Fast relaxation in a fragile liquid under pressure,” *Phys. Rev. Lett.* **80**, 2374–2377 (1998).
- 16 C. Alba-Simionesco, A. Cailliaux, A. Alegría, and G. Tarjus, “Scaling out the density dependence of the  $\alpha$ -relaxation in glass-forming polymers,” *Europhys. Lett.* **68**, 58–64 (2004).
- 17 R. Casalini and C. M. Roland, “Thermodynamical scaling of the glass transition dynamics,” *Phys. Rev. E* **69**, 062501 (2004).
- 18 C. M. Roland, S. Bair, and R. Casalini, “Thermodynamic scaling of the viscosity of van der Waals, H-bonded, and ionic liquids,” *J. Chem. Phys.* **125**(12), 124508 (2006).

- <sup>19</sup>E. R. López, A. S. Pensado, M. J. P. Comuñas, A. A. H. Pádua, J. Fernández, and K. R. Harris, "Density scaling of the transport properties of molecular and ionic liquids," *J. Chem. Phys.* **134**(14), 144507 (2011).
- <sup>20</sup>S. Cheng, M. Musiał, Z. Wojnarowska, A. Holt, C. M. Roland, E. Drockenmüller, and M. Paluch, "Structurally related scaling behavior in ionic systems," *J. Phys. Chem. B* **124**(7), 1240–1244 (2020).
- <sup>21</sup>K. R. Harris and M. Kanakubo, "Self-diffusion, velocity cross-correlation, distinct diffusion and resistance coefficients of the ionic liquid [BMIM][Tf<sub>2</sub>N] at high pressure," *Phys. Chem. Chem. Phys.* **17**, 23977–23993 (2015).
- <sup>22</sup>F. Lundin, H. W. Hansen, K. Adrjanowicz, B. Frick, D. Rauber, R. Hempelmann, O. Shebanova, K. Niss, and A. Matic, "Pressure and temperature dependence of local structure and dynamics in an ionic liquid," *J. Phys. Chem. B* **125**, 2719–2728 (2021).
- <sup>23</sup>H. W. Hansen, F. Lundin, K. Adrjanowicz, B. Frick, A. Matic, and K. Niss, "Density scaling of structure and dynamics of an ionic liquid," *Phys. Chem. Chem. Phys.* **22**, 14169–14176 (2020).
- <sup>24</sup>N. Gnan, T. B. Schröder, U. R. Pedersen, N. P. Bailey, and J. C. Dyre, "Pressure-energy correlations in liquids. IV. 'Isomorphs' in liquid phase diagrams," *J. Chem. Phys.* **131**(23), 234504 (2009).
- <sup>25</sup>T. B. Schröder and J. C. Dyre, "Simplicity of condensed matter at its core: Generic definition of a Roskilde-simple system," *J. Chem. Phys.* **141**, 204502 (2014).
- <sup>26</sup>J. C. Dyre, "Hidden scale invariance in condensed matter," *J. Phys. Chem. B* **118**(34), 10007–10024 (2014).
- <sup>27</sup>N. P. Bailey, U. R. Pedersen, N. Gnan, T. B. Schröder, and J. C. Dyre, "Pressure-energy correlations in liquids. I. Results from computer simulations," *J. Chem. Phys.* **129**(18), 184507 (2008).
- <sup>28</sup>T. S. Ingebrigtsen, T. B. Schröder, and J. C. Dyre, "What is a simple liquid?," *Phys. Rev. X* **2**, 011011 (2012).
- <sup>29</sup>J. P. Hansen and I. R. McDonald, "Statistical mechanics of dense ionized matter. IV. Density and charge fluctuations in a simple molten salt," *Phys. Rev. A* **11**, 2111–2123 (1975).
- <sup>30</sup>T. Schröder, N. P. Bailey, U. R. Pedersen, N. Gnan, and J. C. Dyre, "Pressure-energy correlations in liquids. III. Statistical mechanics and thermodynamics of liquids with hidden scale invariance," *J. Chem. Phys.* **131**, 234503 (2009).
- <sup>31</sup>T. S. Ingebrigtsen, L. Böhling, T. B. Schröder, and J. C. Dyre, "Thermodynamics of condensed matter with strong pressure-energy correlations," *J. Chem. Phys.* **136**, 061102 (2012).
- <sup>32</sup>M. P. Allen and D. J. Tildesley, *Computer Simulation of Liquids* (Oxford University Press, 1987).
- <sup>33</sup>D. Wolf, P. Keblinski, S. R. Phillpot, and J. Eggebrecht, "Exact method for the simulation of Coulombic systems by spherically truncated, pairwise  $r^{-1}$  summation," *J. Chem. Phys.* **110**(17), 8254–8282 (1999).
- <sup>34</sup>S. Toxvaerd and J. C. Dyre, "Communication: Shifted forces in molecular dynamics," *J. Chem. Phys.* **134**(8), 081102 (2011).
- <sup>35</sup>J. S. Hansen, T. B. Schröder, and J. C. Dyre, "Simplistic Coulomb forces in molecular dynamics: Comparing the wolf and shifted-force approximations," *J. Phys. Chem. B* **116**(19), 5738–5743 (2012).
- <sup>36</sup>Y. Zhou, S. Yeh, and G. Stell, "Criticality of charged systems. I. The restricted primitive model," *J. Chem. Phys.* **102**, 5785–5795 (1995).
- <sup>37</sup>P. Atkins and J. de Paula, *Atkins' Physical Chemistry*, 9th ed. (Oxford University Press, 2010).
- <sup>38</sup>H. E. Fischer, A. C. Barnes, and P. S. Salmon, "Neutron and x-ray diffraction studies of liquids and glasses," *Rep. Prog. Phys.* **69**(1), 233–299 (2005).
- <sup>39</sup>N. P. Bailey, T. S. Ingebrigtsen, J. S. Hansen, A. A. Veldhorst, L. Böhling, C. A. Lemarchand, A. E. Olsen, A. K. Bacher, L. Costigliola, U. R. Pedersen, H. Larsen, J. C. Dyre, and T. B. Schröder, "RUMD: A general purpose molecular dynamics package optimized to utilize GPU hardware down to a few thousand particles," *SciPost Phys.* **3**, 038 (2017).
- <sup>40</sup>D. Frenkel and B. Smit, *Understanding Molecular Simulation: From Algorithms to Applications*, 2nd ed., Computational Science Series Vol. 1 (Academic Press, 2002), ISBN: 978-0-12-267351-1.
- <sup>41</sup>A. B. Bhatia and D. E. Thornton, "Structural aspects of the electrical resistivity of binary alloys," *Phys. Rev. B* **2**, 3004–3012 (1970).
- <sup>42</sup>N. P. Bailey, U. R. Pedersen, N. Gnan, T. B. Schröder, and J. C. Dyre, "Pressure-energy correlations in liquids. II. Analysis and consequences," *J. Chem. Phys.* **129**, 184508 (2008).
- <sup>43</sup>Y. Rosenfeld, "Relation between the transport coefficients and the internal entropy of simple systems," *Phys. Rev. A* **15**, 2545–2549 (1977).
- <sup>44</sup>J. C. Dyre, "Perspective: Excess-entropy scaling," *J. Chem. Phys.* **149**, 210901 (2018).
- <sup>45</sup>M. Dzugutov, "A universal scaling law for atomic diffusion in condensed matter," *Nature* **381**, 137–139 (1996).
- <sup>46</sup>N. Gnan, G. Das, M. Sperl, F. Sciortino, and E. Zaccarelli, "Multiple glass singularities and isodynamics in a core-softened model for glass-forming systems," *Phys. Rev. Lett.* **113**, 258302 (2014).
- <sup>47</sup>J. H. R. Clarke, W. Smith, and L. V. Woodcock, "Short range effective potentials for ionic fluids," *J. Chem. Phys.* **84**, 2290 (1986).
- <sup>48</sup>L. Costigliola, private communication (2020).
- <sup>49</sup>L. Böhling, T. S. Ingebrigtsen, A. Grzybowski, M. Paluch, J. C. Dyre, and T. B. Schröder, "Scaling of viscous dynamics in simple liquids: Theory, simulation and experiment," *New J. Phys.* **14**, 113035 (2012).
- <sup>50</sup>J. C. Dyre, "Simple liquids' quasiuniversality and the hard-sphere paradigm," *J. Phys.: Condens. Matter* **28**, 323001 (2016).